Available online at www.sciencedirect.com
SCIENCE DIRECT
Bioorganic & Medicinal Chemistry 14 (2006) 6097–6105
Bioorganic & Medicinal Chemistry

Homology model of RSK2 N-terminal kinase domain, structure-based identification of novel RSK2 inhibitors, and preliminary common pharmacophore

Tam Luong Nguyen,[a,*] Rick Gussio,[b] Jeffrey A. Smith,[c] Deborah A. Lannigan,[c] Sidney M. Hecht,[d] Dominic A. Scudiero,[e] Robert H. Shoemaker[f] and Daniel W. Zaharevitz[b]

[a]*Target Structure-based Drug Discovery Group, SAIC-Frederick, Inc., NCI Frederick, Frederick, MD 21702, USA*
[b]*Target Structure-based Drug Discovery Group, Information Technology Branch, Developmental Therapeutics Program, National Cancer Institute, Frederick, MD 21702, USA*
[c]*Center for Cell Signaling, Departments of Pathology and Microbiology, University of Virginia, Charlottesville, VA 22908, USA*
[d]*Departments of Chemistry and Biology, University of Virginia, Charlottesville, VA 22901, USA*
[e]*Screening Technologies Branch, SAIC-Frederick, Inc., NCI Frederick, Frederick, MD 21702, USA*
[f]*Screening Technologies Branch, Developmental Therapeutics Program, National Cancer Institute, Frederick, MD 21702, USA*

Received 31 March 2006; revised 1 May 2006; accepted 2 May 2006
Available online 24 May 2006

Abstract—Ribosomal S6 kinase 2 (RSK2) is a serine/threonine kinase that plays a role in human cancer and Coffin–Lowry syndrome and is comprised of two nonidentical kinase domains, each domain with its own ATP-binding site. RSK2 can be inactivated by different types of small organic molecules. Potent RSK2 inhibitors include the two classic bisindole maleimide PKC inhibitors, Ro31-8220 and GF109203X, and the natural product SL0101 that was shown to bind specifically to the ATP pocket of the N-terminal domain (NTD). In this paper, we present an atomic model of the RSK2 NTD (residues 68–323), which was built to simultaneously bind the distinctive molecular scaffolds of SL0101, Ro31-8220, and GF109203X. The RSK2 NTD model was used to identify two novel RSK2 inhibitors from the National Cancer Institute open chemical repository and to develop a preliminary structure-based pharmacophore model.
Published by Elsevier Ltd.

1. Introduction

The p90 ribosomal S6 kinases (RSKs) are a family of serine/threonine kinases. While RSK is characterized by four isoforms (RSK1–4), RSK2 has been the focus of considerable attention because it was shown to be overexpressed in human breast cancer,[1,2] and may be linked to human prostate cancer[3] due to its role as an important downstream effector of mitogen-activated protein kinase (MAPK).[4] In addition, mutations in the RSK2 gene are associated with Coffin–Lowry syndrome (CLS), a rare disorder characterized by mental retardation and dysmorphism.[5]

RSK2 consists of two non-identical kinase domains, each with its own ATP-binding site. The N-terminal domain (NTD) is similar to p70 S6 kinase (p70 S6K) and protein kinase C (PKC), while the C-terminal domain is similar to calcium/calmodulin protein kinases.[6] RSK can be inactivated by different small molecules. Two pyrrolo[2,3-d] pyrimidine derivatives have been reported to be irreversible inhibitors of RSK2 CTD.[7] Ro31-8220 **1**[8] and GF109203X **2**,[9] which are two classic bisindole-maleimides PKC inhibitors, are also potent inhibitors of RSK2 with IC_{50}'s of 36 and 310 nM, respectively.[10] Because of the sequence similarity between the PKC and RSK2 NTD, it is reasonable to assume that **1** and **2** bind at the ATP pocket in RSK2 NTD. Finally, the kaempferol-glycoside SL0101 **3**,[11] which was obtained from the tropical plant *Forsteronia refracta*, inhibited RSK2 NTD with an IC_{50} of 89 nM, and exhibited remarkable specificity for RSK relative to other similar kinases, and is competitive with ATP.[2]

Keywords: Ribosomal S6 kinase 2; Homology model; ATP-binding site; Virtual screening; Ligand docking; Pharmacophore.
* Corresponding author. Tel: +1 301 846 6035; fax: +1 301 846 6106; e-mail: nguyent@mail.ncifcrf.gov

0968-0896/$ - see front matter Published by Elsevier Ltd.
doi:10.1016/j.bmc.2006.05.001

Although RSK2 is a therapeutic target, its three-dimensional structure has not yet been determined. Here we present an atomic model of RSK2 NTD (residues 68–323) that was used to identify two novel RSK2 NTD inhibitors from the National Cancer Institute (NCI) open chemical repository. Additionally, the RSK2 NTD model was used to propose binding models and to develop preliminary pharmacophore model for RSK2 inhibition.

2. Results and discussion

2.1. Construction of RSK2 NTD model

The molecular model of RSK2 NTD was constructed in two stages. The first stage involved building a structurally reasonable RSK2 NTD model that was both energetically and hydropathically refined, and the second stage centered on fine tuning the RSK2 NTD model to be experimentally consistent, particularly with published reports of RSK2 inhibition by compounds **1**–**4** (Fig. 1).

In the first stage, an initial homology model of RSK2 NTD (residues 68–323) was constructed, using the 2.0 Å X-ray structure of PKA (Protein Kinase A) complexed with phosphoaminophosphonic acid-adenylate ester (ANP) (PDB code 1CDK)[12] as a template. Since the autophosphorylation of Ser227 in RSK2 is linked to maximal enzyme activity,[13] Ser227 in the model was phosphorylated. The disallowed torsion angles and highly unfavorable atom–atom interactions were corrected using an integrated modeling methodology, as previously described.[14] The initial RSK2 NTD model possessed the overall structure of a kinase, but unfortunately, its ATP-binding site has not been optimized for binding by small organic molecules. Since the structures of kinases are highly dynamic, the ATP-binding site of RSK2 is amenable to ligand-induced conformational changes. For RSK2, what are these structural changes? To address this question, we used the molecular structures of **1**–**4** to define the three-dimensional structure of the ATP-binding site in RSK2 NTD. However, structural refinement of the ATP-binding site is complicated by the fact that the bioactive conformations of **1**–**4** have not been determined and their structure–activity relationships have not been fully elucidated.

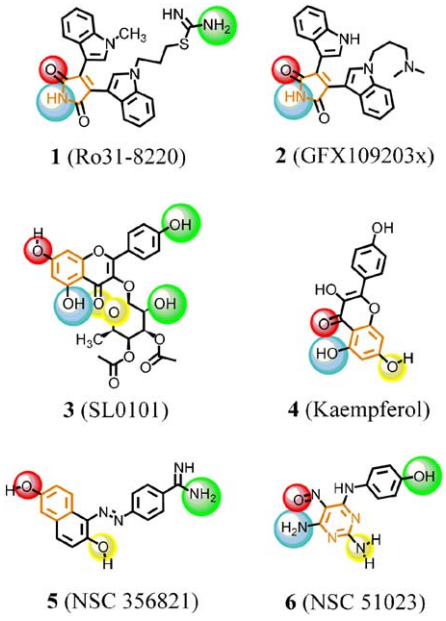

Figure 1. Chemical structures of **1**–**6** with their common names given in parentheses. The red, yellow, cyan, and green spheres represent pharmacophoric points A1, A2, D1, and D2, respectively. The orange bond lines denote pharmacophoric point R1. Points A1 and A2 are hydrogen bond acceptors; points D1 and D2 are hydrogen bond donors; R1 is a planar group.

In the next stage, we optimized the RSK2 NTD model for ligand binding by **1**–**4**. For this, there are two possible strategies. In the first approach, because **1**–**4** are characterized by two structural classes (the bisindole maleimide scaffold for **1** and **2**, and the kaempferol motif for **3** and **4**), two different RSK2 NTD models may be constructed, one to suit **1** and **2**, a second to fit **3** and **4**. A second approach is to construct a common RSK2 NTD model for **1**–**4**, a task that involves canvassing large conformational landscapes for overlap. Because it affords greater potential in structure-based lead discovery, a common RSK2 NTD model for **1**–**4** was constructed.

To overcome the computational challenge, we built a common RSK2 NTD model using a stepwise strategy. To begin, **1** was manually docked into the RSK2 NTD model. Because **1** and ATP have markedly different molecular structures, it was not unexpected that **1** displayed severe steric clashes with RSK2. In order to relieve these steric clashes, it was necessary to expand the molecular volume of the ATP-binding site. The 2.50 Å X-ray structure of PDK1 (3-phosphoinositide-dependent protein kinase-1) in complex with **2** (PDB code 1UU8)[15] was used as a template for directing these conformational changes. This involved the rigid-body movement of structural elements using constrained molecular dynamics. Iterative cycles of simulations were performed until the conformational changes in RSK2 NTD and **1** converged asymptotically on zero. In the next step, **2** was docked into the RSK2 NTD:**1** model, and using a similar protocol as for **1**, the structures and interactions of RSK2 NTD and **2** were hydropathically and energetically refined. Because of the structural similarity between **1** and **2**, RSK2 NTD did not undergo significant conformational changes. Subsequently, compound **3** was manually docked into the ATP-binding site. To retain the ability of the RSK2 NTD model to bind the bisindole maleimide moiety, **1** and **2** were not removed from the ATP-binding site during this second segment. Instead, while the atoms of **1** and **2** were fixed in Cartesian space, the interactions between **3** and RSK2 NTD were optimized, leading to major conformational changes in the triphosphate region of the ATP-binding site. Similarly, **4** was docked, and the complex was refined. Removal of compounds **1**–**4** from the ATP-binding site gave the final RSK2 NTD model. Compounds **1**–**4** were re-docked into the final RSK2 NTD model and energy minimized to produce their respective binding models.

2.2. Overall structure of RSK2 NTD model

Consistent with the PKA template structure, the RSK2 NTD model is bilobal with the ATP-binding site occupying the cleft between the two lobes (Fig. 2A). The small lobe is formed by the N-terminal part of the peptide sequence, and has a three-dimensional structure that is comprised of a helix and a five-stranded antiparallel β-sheet, while the large lobe is formed by the C-terminal of the peptide sequence and has a molecular structure that contains a three-stranded antiparallel β-sheet and a four-helix bundle (Fig. 2B).

Figure 2C shows that the initial RSK2 NTD homology model generated by the Homology module of InsightII closely resembles the template PKA X-ray structure but that the final RSK2 NTD model is significantly different from both the initial RSK2 NTD model and the template PKA structure. The initial and final RSK2 NTD models have a root mean square (r.m.s.) deviation of 3 Å. Because the initial and final RSK2 NTD models have the same secondary structural elements, the opening and closing of RSK2 NTD are mostly due to conformational shifts of the structural elements. Structural analysis indicates that the glycine-rich flap, which forms a portion of the ATP-binding site, undergoes a major conformational shift (Fig. 2C). As with other kinases,[16] the catalytic activity of RSK2 may be linked to the opening and closing of its ATP-binding site. ATP binds to the closed RSK2 state, while small-molecule ligands, which are usually more rigid and larger than ATP, bind to the more open RSK2 conformation.

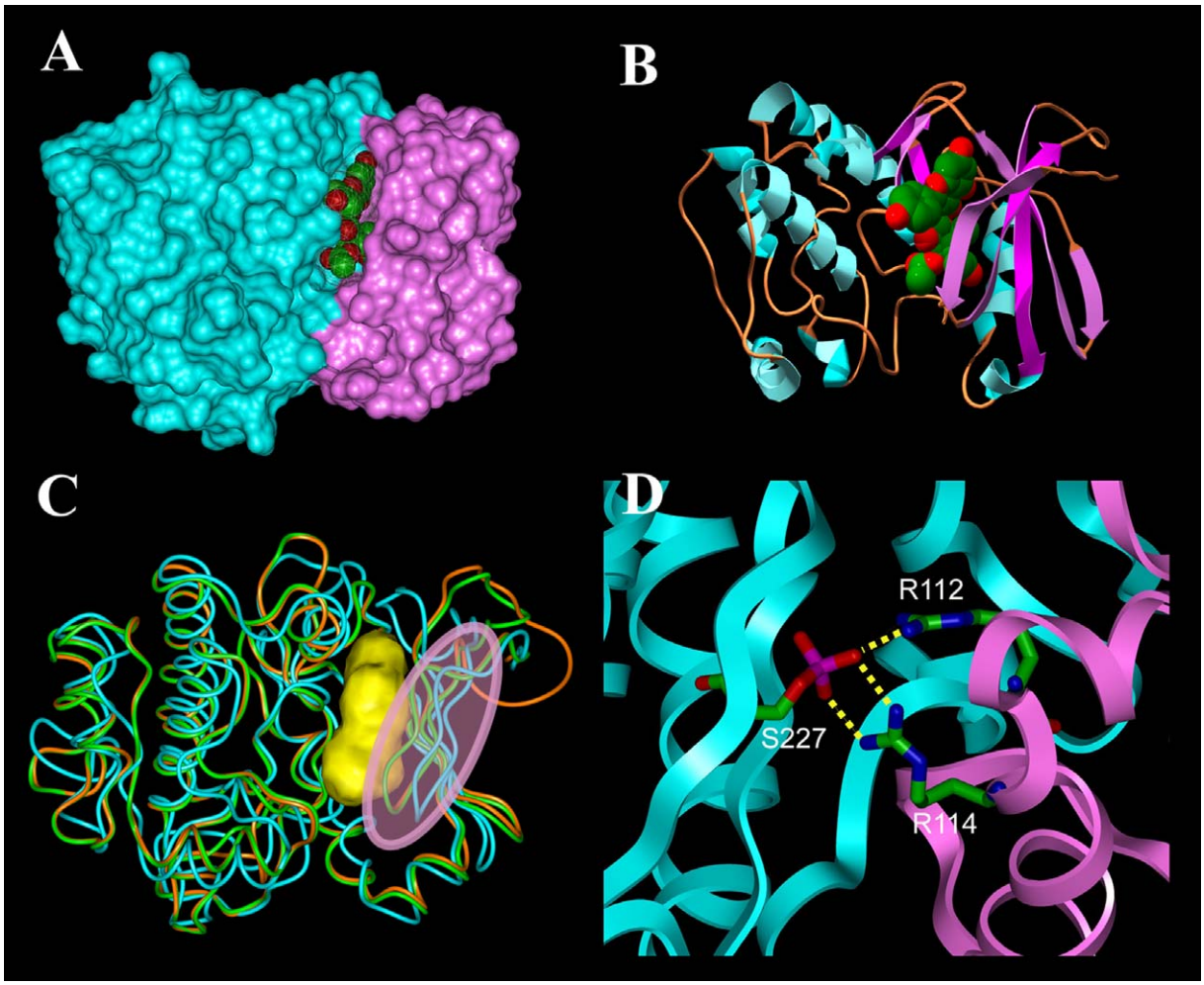

Figure 2. Structure of the RSK2 NTD model. (A and B) RSK2 NTD:SL0101 model. Bound at the cleft between the two lobes, SL0101 is drawn in CPK with carbon atoms colored green and oxygen atoms colored red. Hydrogen atoms are not shown for clarity. (A) RSK2 NTD is rendered as a solid surface with the small lobe colored purple and the large lobe colored cyan. (B) The RSK2 NTD structure is rendered in ribbon with sheet structures colored cyan, helical structures purple, and loop structures orange. (C) Superimposition of the template PKA X-ray structure (PDB code 1CDK), the initial homology model of RSK2 NTD generated from the Homology module of InsightII, and the final hydropathically refined and experimentally consistent RSK2 NTD. The structures are rendered as rounded ribbon with PKA colored green, the initial RSK2 model in orange, and the final RSK2 model in cyan. The yellow surface outlines the relative position of ATP in all three structures, and the transparent oval highlights the glycine-rich flap. (D) Structural basis for the Arg114Trp mutation in RSK2 associated with Coffin–Lowry syndrome (CLS). The RSK2 NTD model is rendered as ribbon with residues in the small lobe colored purple and those in the large lobe colored cyan. Residues Arg112, Arg114, and phosphorylated Ser227 (pSer227) are also drawn as thick sticks with carbon atoms colored green, nitrogen atoms blue, oxygen atoms red, and phosphate atoms purple. Hydrogen atoms are not shown. Hydrogen bonds are shown as yellow dashed lines.

2.3. Structural basis of RSK2 mutations associated with Coffin–Lowry syndrome

Mutations in the RSK2 gene have been associated with the human Coffin–Lowry syndrome (CLS), a disorder that is characterized by severe psychomotor retardation, facial and digital dysmorphisms, and progressive skeletal deformation.[17] Among the RSK2 inactivating-mutations are Gly75Val and Ser227Ala.[18] Previous bioinformatics analysis of protein databases revealed that Gly75 is within the putative ATP-binding site of RSK2 and that Ser227 is the autophosphorylation site located in the activation loop.[18] Because of its topology, the biological importance of Gly75 is evident, even in the absence of an atomic model. However, Ser227 is located outside of the ATP-binding site and is not involved in the ATP-phosphoryl transfer onto the substrate. Accordingly, the biological role of Ser227 is not as apparent. For Ser227 and other RSK2 inactivating-mutations, the RSK2 NTD model may afford critical insights. For instance, the Arg114Trp mutation of RSK2 has been identified in several patients with CLS. Previous protein database analysis showed that Arg114 is located outside of the ATP-binding site in a conserved region of the protein.[19] In the RSK2 NTD model, Arg114 is just outside of the ATP-binding site, and is part of the helix in the small lobe. The guanidinium group of Arg114 is hydrogen bonded to the phosphate group of pSer227 which is part of the large lobe (Fig. 2D). The Arg114–pSer227 hydrogen bond is complemented by a similar hydrogen bond between Arg112 and pSer227. Since the small and large lobes are weakly associated, these two strong hydrogen bonds may provide critical stability to the tertiary structure of RSK2. In the Arg114Trp mutant, one or both of these hydrogen bonds is lost, which may destabilize the tertiary structure of RSK2 and lead to RSK2 inactivation.

2.4. Architecture of the ATP-binding site

Figure 3 shows a side-by-side view of the ATP-binding site in the RSK2 NTD model and in the PKA:ANP X-ray structure. The two ATP-binding sites contain the three characteristic regions of a kinase: an adenine, a ribose and a triphosphate region. The PKA structure represents a closed kinase conformation that is bound to ATP, and the RSK2 NTD model represents a more open conformation that is optimized for binding small organic molecules.

In the adenine region of the RSK2 NTD model, the backbone oxygen atom of Asp148, the backbone nitrogen atom of Leu150 and the hydroxyl oxygen atom of Thr210 are capable of forming hydrogen bonds to the bound ligand. The corresponding residues in PKA are Glu121, Val123, and Thr183, respectively. In addition, the plane representing the purine motif is characterized by hydrophobic clusters on both sides. In the RSK2 NTD model, Leu74 and Val82 are on one side and Leu200 is on the other side. The purine plane in PKA has Leu49 and Val57 opposite Leu173.

In the ribose region of the RSK2 NTD model, the side-chain carboxylate of Asp154 and the backbone oxygen atom of Glu197 are positioned to form hydrogen bonds. The corresponding residues in PKA are Glu127 and Glu170, respectively. Although not bound to ATP, the triphosphate region of the RSK2 NTD model has five potential hydrogen bonding sites. These are the backbone nitrogen atoms of Ser78, Phe79, and Gly80, and the side-chain amino nitrogen atoms of Lys100 and Lys195. The corresponding residues in PKA are Ser53, Phe54, Gly55, Lys72, and Lys168, respectively. Mutational studies of RSK2 indicate that Lys100 is essential

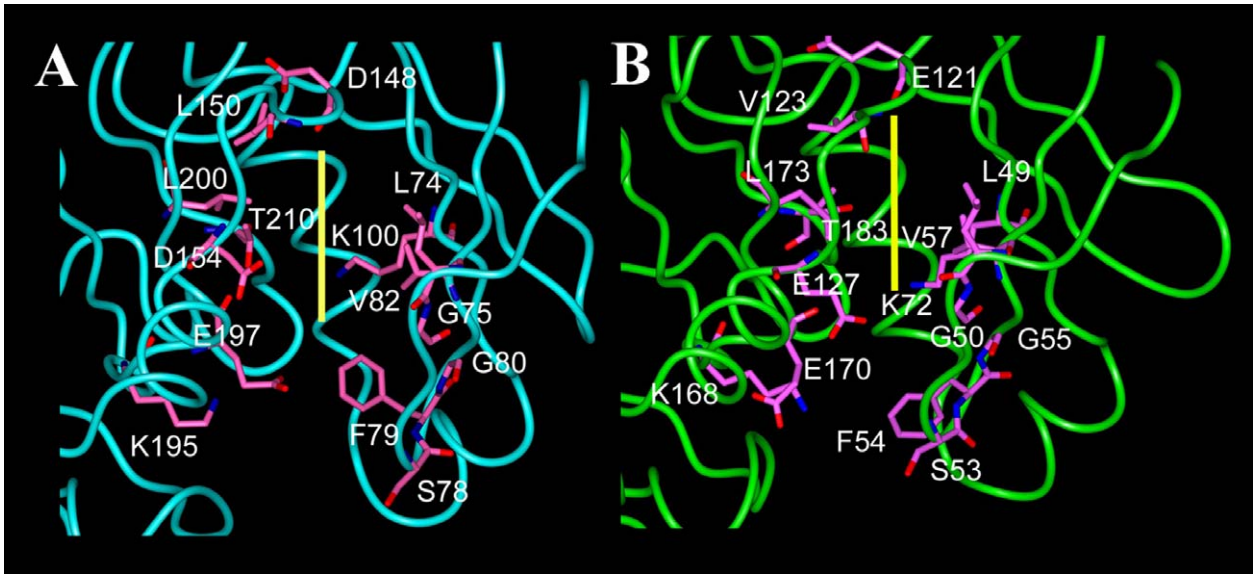

Figure 3. Comparison of ATP-binding site in RSK2 NTD model (A) and template PKA X-ray structure (B). The structures are rendered as round ribbon with the RSK2 NTD colored cyan and the PKA template structure colored green. The key residues in each site are also rendered stick and colored purple in both RSK2 and PKA structures. The yellow line represents the plane of the purine ring that separates the two hydrophobic sides of the ATP-binding site.

to kinase activity,[20] and this is supported by the RSK2 NTD model that has the terminal –NH of Lys100 forming a strong hydrogen bond to an α-phosphate oxygen of ATP (data not shown).

2.5. Structure-based lead discovery

The ATP-binding site of the RSK2 NTD model was used to virtually screen a subset of compounds from NCI open chemical repository for new RSK2 inhibitors. The subset contained NCI compounds with inventory of greater than 1 g, since these compounds are obtainable for testing. Besides their steric and electronic complementarity to the ATP-binding site, compounds were also selected for their unique chemical structures relative to known RSK2 inhibitors. Nineteen candidate compounds were identified and submitted for testing. RSK2 inhibition was measured using a fluorescence-based assay.

Among the 19 compounds tested, two were identified as lead compounds, providing a remarkably high hit rate of 10%. These compounds are NSC 356821 **5** and NSC 51023 **6**, which have IC_{50}'s of 1 and 28 μM for RSK2, respectively (Fig. 1). Compound **5** is a dihydroxylnapthalene derivative and **6** is diaminonitrosopyrimidine derivative. Because both **5** and **6** have distinctly different chemical structures from one another and to any published RSK inhibitor, their identification as potent RSK2 inhibitors confirms the utility of the RSK2 NTD model in de novo lead discovery.

2.6. Binding models

Figure 4 shows the individual binding models of **1**–**6**. Each ligand establishes multiple hydrogen bonds to RSK2. The frequency of hydrogen bonds is as follows: (1) all six inhibitors are capable of forming hydrogen bonds with Leu150 with a calculated distance range of 2.4–3.6 Å, (2) five can form hydrogen bonds to Asp148 with a distance range of 2.4–3.7 Å, and (3) four can directly hydrogen bond to Glu197 with a distance range of 2.6–2.8 Å, (4) four can potentially hydrogen bond Thr210 with a distance range of 3.5–4.2 Å, and (5) one can hydrogen bond to Glu154 with a distance of 2.8 Å. Although some of these hydrogen bond distances are greater than expected for typical hydrogen bonds, the plasticity of the RSK2 NTD due to its function as a kinase may allow these groups to establish hydrogen bonds.

While **1** and **2** form similar hydrogen bonds using their maleimide groups, their bisindole groups form different hydrogen bonds. The unsubstituted indole group of **2** is hydrogen bonded to the carboxylate group of Glu154. In contrast, since its indole nitrogen atom is methylated, **1** cannot directly hydrogen bond to Glu154. Additionally, whereas the isothiourea of **1** can hydrogen bond to the side-chain carboxylate of Glu197 via its terminal –NHs, the dimethylamino group of **2** is not hydrogen bonded. Compounds **1** and **2** have reported IC_{50} values of 36 and 310 nM for RSK2, respectively.[10] Because the isothiourea-carboxylate hydrogen bond of **1** is a stronger interaction than the

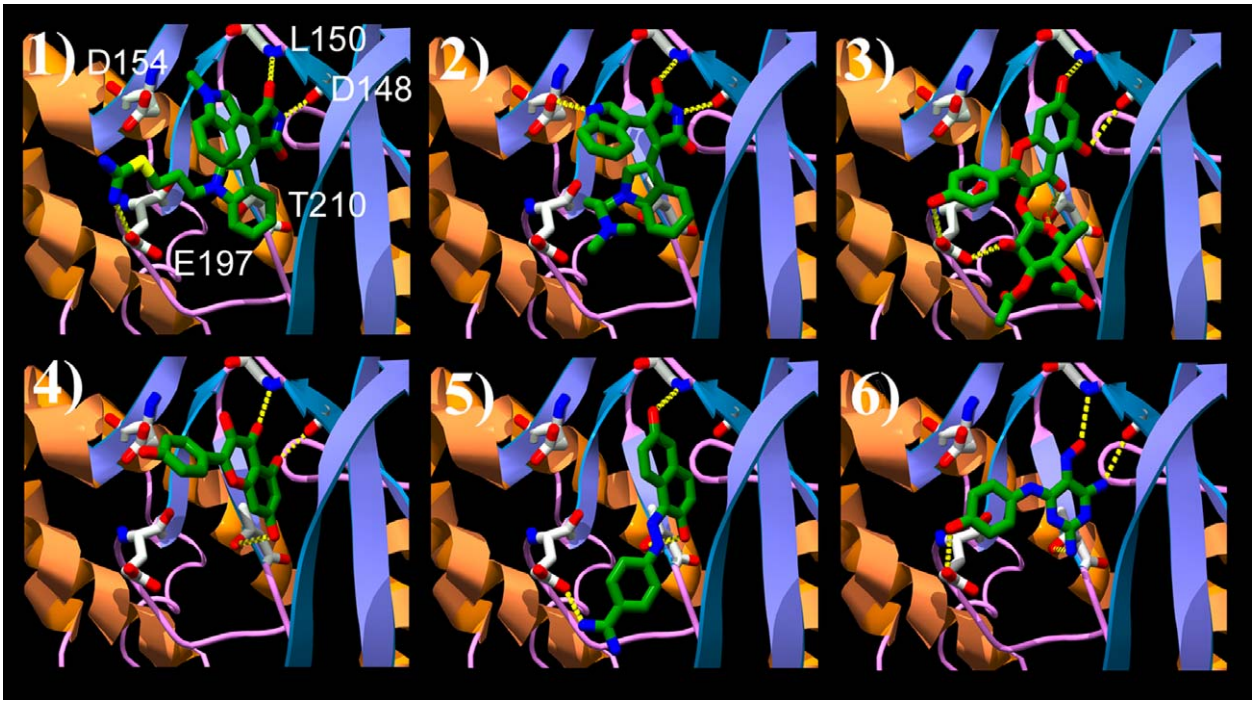

Figure 4. Binding models of **1**–**6**. RSK2 NTD is rendered in ribbon with helical structures colored orange, sheet structures cyan, and loop structures purple. Residues Asp148, Leu150, Asp154, Glu197, and Thr210, and compounds **1**–**6** are shown in stick with the carbon atoms of RSK2 NTD colored white and the carbon atoms of **1**–**6** green. Nitrogen atoms are colored blue and oxygen atoms red. Hydrogen atoms are not depicted for clarity. Yellow dashed lines indicate potential intermolecular hydrogen bonds. The compound number is at the top left corner of each panel.

indole-carboxylate hydrogen bond of **2**, this may explain their difference in activity.

The kaempferol moieties of **3** and **4** have different orientations in the ATP-binding site. For **3**, the 5,7-dihydroxyl moiety is hydrogen bonded to Asp148 and Leu150, and its carbonyl group is hydrogen bonded to Thr210. In contrast, the kaempferol moiety of **4** is aligned nearly 90° relative to **3** with its carbonyl and 5-hydroxyl groups hydrogen bonded to Asp148 and Leu150, respectively, and its 7-hydroxyl group hydrogen bonded to Thr210. Additionally, because of its larger size, compound **3** forms significantly more intermolecular contacts than **4**. The 4′-hydroxyl and rhamnose hydroxyl groups of **3** can simultaneously form hydrogen bonds to the carboxylate group of Glu197, and the carbonyl oxygen and rhamnose ring oxygen atoms of **3** can both form hydrogen bonds to the hydroxyl group of Thr210. Favorable hydrophobic contacts include interactions between the rhamnose methyl group of **3** against the alipathic side chains of Val82 and Lys100. These additional hydrogen bonds and hydrophobic contacts may explain the greater inhibitory activity of **3** relative to **4**, which have IC_{50}'s of 89 nM and 15 μM, respectively.[2]

While the chemical structures of **5** and **6** are distinct from **1** to **4**, these two compounds can form similar hydrogen bonds with RSK2. For **5**, three hydrogen bonds are evident in its binding model. The hydroxyl groups of **5** are hydrogen bonded to Leu150 and Thr210, and its amidine group forms a strong hydrogen bond with the carboxylate group of Glu197. For **6**, four hydrogen bonds are possible. The 6-amino nitrogen and nitroso oxygen atoms of **6** are hydrogen bonded to Asp148 and Leu150, respectively. These hydrogen bonds are complemented by hydrogen bonds between the phenolic oxygen atom of **6** and the carboxylate group of Glu197, and between the 2-amino and the hydroxyl group of Thr210. While **6** forms one additional intermolecular hydrogen bond compared to **5**, it is a weaker RSK2 inhibitor, as evident by IC_{50}'s of 1 and 28 μM for **5** and **6**, respectively. This difference in inhibitory activity may be explained by the fact that the hydrogen bonds between RSK2 and **6** are not as strong as those involving **5**. Because of their topology, the 6-amino and nitroso groups of **6** are not optimally positioned for forming hydrogen bonds with Asp148 and Leu150, respectively. This is indicated by the hydrogen bond distances of 3.53 and 3.64 Å for 6-amino and nitroso hydrogen bonds, respectively. Additionally, the higher heteroatom content of **6** may make it less favorable in the hydrophobic pocket of the ATP-binding site.

2.7. Preliminary common pharmacophore

The binding models of **1**–**6** were used to construct a preliminary pharmacophore model. The consistent structural features and recurring protein–ligand interactions provided the basis for the pharmacophoric points. Five pharmacophoric points were identified: two hydrogen bond donors (D1 and D2), two hydrogen bond acceptors (A1 and A2), and a planar group (R1). The pharmacophoric points were color coded into the chemical structures of **1**–**6** in Figure 1. For **3**, multiple heteroatoms represent points A2 and D2. In the binding model of **3**, the carbonyl and rhamnose ring oxygen atoms can both form hydrogen bonds to the hydroxyl group of Thr210, and therefore, may both be characterized by point A2. Similarly, the 4′-hydroxyl and rhamnose hydroxyl oxygen atoms of **3** can hydrogen bond to the side-chain carboxylic acid of Glu197, and therefore, may be described by point D2.

The pharmacophoric points A1 and R1 are common to all six compounds, and the hydrogen bond donor D1 is common to five compounds with the one missing compound being NSC 356821. This suggests that points A1, D1, and R1 are essential for RSK2 inhibition. Other kinase inhibitors such as the well-studied tyrosine kinase inhibitor Gleevec[21] are also characterized by these three pharmacophoric features.

The two remaining pharmacophoric points A2 and D2 may contribute to binding affinity and specificity. The two lead compounds **5** and **6** possess pharmacophoric points A2 and D2. However, compound **5** lacks the pharmacophoric points D1. Because of this, chemical modifications that would give **5** a hydrogen bond donor moiety at 5-position of the naphthalene ring is predicted to increase the compound's inhibitory property.

In summary, we have constructed an energetically and hydropathically refined molecular model of RSK2 NTD with an ATP-binding site optimized for binding multiple structural classes of RSK2 inhibitors. The RSK2 NTD model was used to identify two novel RSK2 inhibitors with IC_{50}'s of 1 and 28 μM from the NCI open chemical repository, demonstrating its utility in lead discovery. Additionally, the RSK2 NTD model may provide structural insights into disease-related mutations.

3. Experimental

3.1. General

All simulations were performed using the CFF91 force-field with the nonbonded interaction limited to 13 Å and a distance-dependent dielectric constant using Discover 3.0 (Accelrys, San Diego, CA). The HINT program (eduSoft, Richmond, VA) was used to evaluate the hydropathic quality of the interatomic interactions, as previously described.[22]

3.2. Structures of small molecules

The structures of **1**–**6** were constructed in the Biopolymer module and energy minimized in Discover using the CFF91 force-field and the VA09A algorithm with a convergence criterion of 1.0×10^{-3} kcal/mol.

3.3. Modeling of RSK2 NTD

The RSK2 NTD model was constructed in two stages. The first stage involved building a structurally reason-

able RSK2 NTD model that was both energetically and hydropathically refined, while the second stage centered on fine tuning the RSK2 NTD model to be experimentally consistent, particularly with published data showing RSK2 inhibition by **1**–**4** (Fig. 1). Because of the complexity associated with modeling a common RSK2 NTD structure for binding **1**–**4**, the RSK2 NTD model was achieved stepwise.

In the first stage, the 2.00 Å X-ray structure of PKA (PDB code 1CDK) in complex with ANP, a close analogue of ATP, was selected as the template for the RSK2 NTD model. The sequences of PKA and RSK2 NTD (residues 68–323) were aligned using the alignment method in the Homology module, and the Modeler program was used to generate a RSK2 NTD model based on this sequence alignment. Structural analysis of the RSK2 NTD model using the Procheck[23] and HINT programs revealed residues in the disallowed regions of the Ramachandran plot, and unfavorable atom–atom interactions.

Consequently, the RSK2 NTD model was subjected to energetic and hydropathic refinement to remove disallowed torsion angles and unfavorable atom–atom interactions.[14] To maintain the structural integrity of the ATP-binding site during simulations, an ATP molecule was manually docked into the ATP-binding site, and its position was fixed in Cartesian space. In addition, Ser227, which is a phosphorylation site in RSK2, was phosphorylated in the model. Structural refinement involved iterative cycles of: (1) manual adjustment of the torsion angle until it was located in one of the allowed regions, (2) constrained molecular dynamics simulations that were performed for 500 fs in 500 steps with a time step of 1 fs at 300 k and that incorporated distance constraints to incrementally separate the two atoms involved in the unfavorable interactions, and (3) energy minimization involving up to 5000 steps of Fletcher–Powell optimization until the norm of the gradient was <1.0 kcal/mol Å^2. The RSK2 NTD model was refined to the hydropathic quality of the PKA:ANP template X-ray structure. While the RSK2 NTD model was structurally reasonable, preliminary docking studies showed that the conformation of its ATP-binding site was not optimal for binding **1**–**4** (Fig. 1).

In the second stage, the RSK2 NTD model was refined to be biochemically reasonable. The RSK2 NTD model was refined to hydropathically accommodate **1** in its ATP-binding site. Compound **1** was docked into the ATP-binding site with its maleimide functionality of **1** functioning as the bioisostere of the ATP purine ring. The ATP molecule was removed. Compound **1** displayed severe steric clashes with RSK2, and in order to relieve these steric clashes, it was necessary to expand the molecular volume of the ATP-binding site. The 2.50 Å X-ray structure of PDK1 in complex with **2** (PDB code 1UU8)[15] was used as a template for directing this conformational change. This involved the rigid-body movement of the structural elements using constrained molecular dynamics, while **1** was fixed in Cartesian space. In the next stage, **1** was re-docked, and while RSK2 NTD was fixed in Cartesian space, molecular mechanics energy minimization was employed to find the nearest local minima of **1** in the ATP-binding site. Iterative cycles of refinement were performed until the conformational changes in RSK2 NTD and **1** asymptotically approached zero. Compound **2** was manually docked into the RSK2 NTD:**1** model using **1** as a template. A similar refinement was performed on RSK2 NTD:**2**. Afterwards, **1** was re-docked into the RSK2 NTD to establish the capability of the RSK2 NTD with **1**. In the second stage, RSK2 NTD was refined to fit **3**. Compound **3** was manually docked into the ATP-binding site of the RSK2 NTD:**1** model with its 5,7-dihydroxyl group functioning as the bioisostere of the maleimide functionality of **1** and **2**. Compound **3** extends to the triphosphate region of the ATP-binding site and provides the template for the conformation of this region. During the refinement of the RSK2 NTD:**3** model, **1** and **2** were kept in the ATP-binding site, the positions of their atoms fixed in Cartesian space. The hydropathic quality of the interactions between RSK2 NTD and **3** was refined. Afterwards, **4** was docked into the RSK2 NTD model and its interactions with RSK2 were energetically and hydropathically refined. In the end, removal of **1**–**4** from the ATP-binding site gave the final RSK2 NTD model.

3.4. Three-dimensional query of the NCI chemical repository

The RSK2 NTD protein model was used to virtually screen the NCI open chemical repository for potential ATP-binding site inhibitors. The pharmacophore model and the molecular volume of the ATP-binding site in the RSK2 NTD model were used to identify 837 compounds in the NCI repository as potential RSK2 inhibitors. Detailed molecular docking studies of the 837 compounds indicated that 52 possessed suitable steric and electrostatic fit to the ATP-binding site to be potent RSK2 inhibitors. Of the 52 compounds, 22 had sufficient inventory in the NCI repository to be obtainable for biological testing. Nineteen compounds were actually obtained and tested, producing the two lead compounds identified in this paper.

3.5. Biological assays

Kinase activity was assayed using recombinant RSK2 enzyme, which was prepared as previously described.[24] Fluoroscein-labeled peptide substrate for RSK2 and IMAP™ beads for capturing phosphorylated product were purchased from Molecular Devices. These reagents were combined in assay buffer containing 10 μM ATP and test compounds in 384-well Greiner (Matrical) black plates (20 μL final volume). Phosphorylated substrate was detected by fluorescence polarization spectroscopy after binding to IMAP™ beads. Half-maximal inhibitory concentrations (IC_{50}) were read from concentration-response curves by linear interpolation. Using this assay, SL0101 had an IC_{50} of 350 nM. Compounds **5** and **6** were identified as new RSK2 NTD inhibitors with IC_{50}'s of 1 and 28 μM, respectively.

3.6. Binding models

Compounds **1**–**6** were docked into the ATP-binding site of the RSK2 NTD model, using the maleimide and 5,7-dihydroxyl moieties as bioisosteres of the ATP purine ring, and were subjected to energy minimization, while RSK2 NTD was held fixed in Cartesian space. Consistent structural features and recurring protein–ligand interactions were identified in the binding models and were used to develop a structure-based pharmacophore.

Acknowledgments

This project has been funded in whole or in part with Federal funds from the National Cancer Institute, National Institutes of Health, under Contract NO1-CO-12400 and by the Intramural Research Program of the NIH, National Cancer Institute, Center for Cancer Research. The content of this publication does not necessarily reflect the views or policies of the Department of Health and Human Services, nor does mention of trade names, commercial products, or organization imply endorsement by the U.S. Government.

Supplementary data

Supplementary data associated with this article can be found, in the online version, at doi:10.1016/j.bmc.2006.05.001.

References and notes

1. Clark, D. E.; Errington, T. M.; Smith, J. A.; Frierson, H. F., Jr.; Weber, M. J.; Lannigan, D. A. The serine/threonine protein kinase, p90 ribosomal S6 kinase, is an important regulator of prostate cancer cell proliferation. *Cancer Res.* **2005**, *65*, 3108–3116.
2. Smith, J. A.; Poteet-Smith, C. E.; Xu, Y.; Errington, T. M.; Hecht, S. M.; Lannigan, D. A. Identification of the first specific inhibitor of p90 ribosomal S6 kinase (RSK) reveals an unexpected role for RSK in cancer cell proliferation. *Cancer Res.* **2005**, *65*, 1027–1034.
3. Gioeli, D.; Mandell, J. W.; Petroni, G. R.; Frierson, H. F., Jr.; Weber, M. J. Activation of mitogen-activated protein kinase associated with prostate cancer progression. *Cancer Res.* **1999**, *59*, 279–284.
4. Smith, J. A.; Poteet-Smith, C. E.; Malarkey, K.; Sturgill, T. W. Identification of an extracellular signal-regulated kinase (ERK) docking site in ribosomal S6 kinase, a sequence critical for activation by ERK in vivo. *J. Biol. Chem.* **1999**, *274*, 2893–2898.
5. Jacquot, S.; Merienne, K.; De Cesare, D.; Pannetier, S.; Mandel, J. L.; Sassone-Corsi, P.; Hanauer, A. Mutation analysis of the RSK2 gene in Coffin–Lowry patients: extensive allelic heterogeneity and a high rate of de novo mutations. *Am. J. Hum. Genet.* **1998**, *63*, 1631–1640.
6. Jones, S. W.; Erikson, E.; Blenis, J.; Maller, J. L.; Erikson, R. L. A Xenopus ribosomal protein S6 kinase has two apparent kinase domains that are each similar to distinct protein kinases. *Proc. Natl. Acad. Sci. U.S.A.* **1988**, *85*, 3377–3381.
7. Cohen, M. S.; Zhang, C.; Shokat, K. M.; Taunton, J. Structural bioinformatics-based design of selective, irreversible kinase inhibitors. *Science* **2005**, *308*, 1318–1321.
8. Morreale, A.; Mallon, B.; Beale, G.; Watson, J.; Rumsby, M. Ro31-8220 inhibits protein kinase C to block the phorbol ester-stimulated release of choline- and ethanolamine-metabolites from C6 glioma cells: p70 S6 kinase and MAPKAP kinase-1beta do not function downstream of PKC in activating PLD. *FEBS Lett.* **1997**, *417*, 38–42.
9. Alessi, D. R. The protein kinase C inhibitors Ro 318220 and GF 109203X are equally potent inhibitors of MAPKAP kinase-1beta (Rsk-2) and p70 S6 kinase. *FEBS Lett.* **1997**, *402*, 121–123.
10. Roberts, N. A.; Haworth, R. S.; Avkiran, M. Effects of bisindolylmaleimide PKC inhibitors on p90RSK activity in vitro and in adult ventricular myocytes. *Br. J. Pharmacol.* **2005**, *145*, 477–489.
11. Maloney, D. J.; Hecht, S. M. Synthesis of a potent and selective inhibitor of p90 Rsk. *Org. Lett.* **2005**, *7*, 1097–1099.
12. Bossemeyer, D.; Engh, R. A.; Kinzel, V.; Ponstingl, H.; Huber, R. Phosphotransferase and substrate binding mechanism of the cAMP-dependent protein kinase catalytic subunit from porcine heart as deduced from the 2.0 A structure of the complex with Mn^{2+} adenylyl imidodiphosphate and inhibitor peptide PKI(5–24). *EMBO J.* **1993**, *12*, 849–859.
13. Bjorbaek, C.; Zhao, Y.; Moller, D. E. Divergent functional roles for p90rsk kinase domains. *J. Biol. Chem.* **1995**, *270*, 18848–18852.
14. Nguyen, T. L.; Schoehn, G.; Weissenhorn, W.; Hermone, A. R.; Burnett, J. C.; Panchal, R. G.; McGrath, C.; Zaharevitz, D. W.; Aman, M. J.; Gussio, R.; Bavari, S. An all-atom model of the pore-like structure of hexameric VP40 from Ebola: structural insights into the monomer–hexamer transition. *J. Struct. Biol.* **2005**, *151*, 30–40.
15. Komander, D.; Kular, G. S.; Schuttelkopf, A. W.; Deak, M.; Prakash, K. R.; Bain, J.; Elliott, M.; Garrido-Franco, M.; Kozikowski, A. P.; Alessi, D. R.; van Aalten, D. M. Interactions of LY333531 and other bisindolyl maleimide inhibitors with PDK1. *Structure* **2004**, *12*, 215–226.
16. Johnson, D. A.; Akamine, P.; Radzio-Andzelm, E.; Madhusudan, M.; Taylor, S. S. Dynamics of cAMP-dependent protein kinase. *Chem. Rev.* **2001**, *101*, 2243–2270.
17. Hanauer, A.; Young, I. D. Coffin–Lowry syndrome: clinical and molecular features. *J. Med. Genet.* **2002**, *39*, 705–713.
18. Trivier, E.; De Cesare, D.; Jacquot, S.; Pannetier, S.; Zackai, E.; Young, I.; Mandel, J. L.; Sassone-Corsi, P.; Hanauer, A. Mutations in the kinase Rsk-2 associated with Coffin–Lowry syndrome. *Nature* **1996**, *384*, 567–570.
19. Abidi, F.; Jacquot, S.; Lassiter, C.; Trivier, E.; Hanauer, A.; Schwartz, C. E. Novel mutations in Rsk-2, the gene for Coffin–Lowry syndrome (CLS). *Eur. J. Hum. Genet.* **1999**, *7*, 20–26.
20. Chrestensen, C. A.; Sturgill, T. W. Characterization of the p90 ribosomal S6 kinase 2 carboxyl-terminal domain as a protein kinase. *J. Biol. Chem.* **2002**, *277*, 27733–27741.
21. Atwell, S.; Adams, J. M.; Badger, J.; Buchanan, M. D.; Feil, I. K.; Froning, K. J.; Gao, X.; Hendle, J.; Keegan, K.; Leon, B. C.; Muller-Dieckmann, H. J.; Nienaber, V. L.; Noland, B. W.; Post, K.; Rajashankar, K. R.; Ramos, A.; Russell, M.; Burley, S. K.; Buchanan, S. G. A novel mode of Gleevec binding is revealed by the structure of spleen tyrosine kinase. *J. Biol. Chem.* **2004**, *279*, 55827–55832.
22. Kellogg, G. E.; Semus, S. F.; Abraham, D. J. HINT: a new method of empirical hydrophobic field calculation for CoMFA. *J. Comput. Aided Mol. Des.* **1991**, *5*, 545–552.

23. Laskowski, R. A.; MacArthur, M. W.; Thornton, J. M. Validation of protein models derived from experiment. *Curr. Opin. Struct. Biol.* **1998**, *8*, 631–639.

24. Clark, D. E.; Poteet-Smith, C. E.; Smith, J. A.; Lannigan, D. A. Rsk2 allosterically activates estrogen receptor alpha by docking to the hormone-binding domain. *EMBO J.* **2001**, *20*, 3484–3494.